Communication

Electrochemical Performance and Resistance Analysis of $Li_3V_2(PO_4)_3$/C Composite Cathode for Li Ion Battery

SHULAN WANG, XUAN LIU, HUIQING LI, and LI LI

$Li_3V_2(PO_4)_3$/C composites were prepared at different temperatures and assembled as cathodes for Li ion batteries. Their structure and electrochemical properties were properly characterized. The internal and charge transfer resistance of the $Li_3V_2(PO_4)_3$/C cathodes were obtained by simulating the ac impedance spectra with equivalent circuits. The $Li_3V_2(PO_4)_3$/C composite sintered at 1123 K (850 °C) exhibits excellent electrochemical performances because of its smaller internal resistance and charge transfer resistance, as well as faster Li ion inserting/extracting rates.
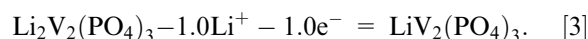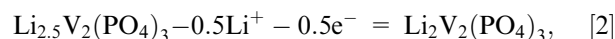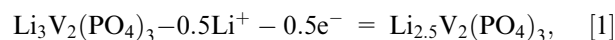

The lithium ion battery (LIB) is considered as a primary sustainable source for energy storage and transfer.[1] Currently, extensive research work is focused on monoclinic $Li_3V_2(PO_4)_3$ as the cathode material for LIB because of its high operating voltage (3.85 V), large theoretical capacity (197 mAh g^{-1}), and safe performance.[2,3] However, the major challenge for $Li_3V_2(PO_4)_3$ is its low electrical conductivity at room temperature. Various efforts have been made to improve its electrical conductivity and electrochemical performance, including supporting with carbon materials,[4–11] narrowing the particle size distribution of $Li_3V_2(PO_4)_3$,[12–14] and doping with metals.[15–26] $Li_3V_2(PO_4)_3$ coated with SiO_2, exhibited significant improvement in electrochemical performance because of the enhanced structural stability and reduced charge transfer resistance of the active material.[27] Xu reported a high-performance $Li_3V_2(PO_4)_3$ cathode material for lithium ion batteries synthesized by the microwave-assisted hydrothermal method followed by a post annealing process.[9] The $Li_3V_2(PO_4)_3$ electrode measured at 10 °C after 500 cycles can deliver discharge capacities of 85.4 mAh g^{-1} with a capacity retention of 99.3 pct in the voltage ranges of 3.0 to 4.3 V. The macroporous $Li_3V_2(PO_4)_3$(LVP) cathode materials prepared *via* a templating method shows initial discharge capacity of 189.4 mAh g^{-1} at 0.1 C in the potential range of 3.0–4.8 V.[10] Structure change of $Li_3V_2(PO_4)_3$ anode was also investigated by constructing a symmetry cell.[28] The result showed that Li can extract/insert reversibly in $Li_3V_2(PO_4)_3$ with a NASICON structure due to the structural strength and flexibility of NASICON framework with the corner-sharing matrix.[28]

The charge/discharge process of $Li_3V_2(PO_4)_3$ in the potential range of 3.0 to 4.3 V can be divided into three steps as shown below:[29–32]

$$Li_3V_2(PO_4)_3 - 0.5Li^+ - 0.5e^- = Li_{2.5}V_2(PO_4)_3, \quad [1]$$

$$Li_{2.5}V_2(PO_4)_3 - 0.5Li^+ - 0.5e^- = Li_2V_2(PO_4)_3, \quad [2]$$

$$Li_2V_2(PO_4)_3 - 1.0Li^+ - 1.0e^- = LiV_2(PO_4)_3. \quad [3]$$

Two lithium ions are inserted/extracted with a theoretical capacity of 133 mAh g^{-1}.[33] Each step consists of two processes, namely, diffusion and charge transfer.[29] The capacity, as well as the capacity rate of $Li_3V_2(PO_4)_3$ cathode, depends on the resistance during the charge/discharge steps. In the present work, $Li_3V_2(PO_4)_3$/C composites were prepared by solid-state reaction with their electrochemical performances as cathodes investigated. The charge transfer resistance of $Li_3V_2(PO_4)_3$/C cathode and the internal resistance of Li ion insertion/extraction in the cathode were obtained *via* simulating the ac impedance spectra with and without overlapping a dc voltage, which provides a fundamental understanding for the charge/discharge process of Li ion and is beneficial for design of high-performance cathodes for lithium ion batteries.

All regents were used as-received without further purification. $Li_3V_2(PO_4)_3$/C composites were prepared by modified solid state reaction. Li_2CO_3, V_2O_5, $(NH_4)_2HPO_4$, and sucrose were mixed in alcohol with a mole ratio of 3.06:2.00:3.00 (Li:V:P) and 1:0.2 ($Li_3V_2(PO_4)_3$:sucrose) in which the ratio of Li and V is over their stoichiometric in $Li_3V_2(PO_4)_3$ for compensating possible loss of lithium source during high temperature processing.[17] The powder mixture was ball-milled at 350 rpm for 5 hours and then dried at 353 K (80 °C) for 3 hours before pelleting. The pellets (25 mm in diameter, 2 mm in thickness) were heated up to 573 K (300 °C) in N_2 atmosphere at a heating rate of 10 °C/minute and then sintered for 5 hours. The samples were cooled down to room temperature and further hand-milled for 3 hours. Finally, these as-prepared pellet powders were pressed and sintered in N_2 atmosphere at 1073 K and 1123 K (800 °C and 850 °C), respectively, for 12 hours.

X-ray diffraction (XRD) patterns were collected using a Philips PW3040/60 diffractometer at a scanning rate of 0.3 deg min^{-1} for 2θ in the range of 10 to 65 deg. SSX-500 scanning electron microscope (SEM) operated at an accelerating voltage of 30 kV was used to analyze

SHULAN WANG, Professor, and HUIQING LI, Graduate Student, are with the Department of Chemistry, School of Science, Northeastern University, Shenyang 110819, P.R. China. XUAN LIU, Research Associate, is with the Department of Materials Science and Engineering, Carnegie Mellon University, Pittsburgh, PA 15213. LI LI, Postdoc Associate, is with the Department of Materials Science and Engineering, Cornell University, Ithaca, NY 14850. Contact-emails: lilicmu@gmail.com, ll644@cornell.edu

surface morphology of the composites. The carbon content in $Li_3V_2(PO_4)_3$/C was measured by a LECO carbon-sulfur analyzer (CS600). The $Li_3V_2(PO_4)_3$/C electrode was prepared by spreading a paste of $Li_3V_2(PO_4)_3$/C, PVDF, and acetylene black (80:10:10 in wt pct) in N-methyl pyrrolidinone on an aluminum foil (20 mm in thickness) by an automatic film coating instrument. The working electrode in the Li ion coil cell (CR2025 type) was dried in vacuum at 393 K (120 °C) for 12 hours and then cut into circles (6 mm in diameter) with subsequent pressing at 15 MPa. A lithium foil is used as both the counter and the reference electrode. 1 mol L^{-1} $LiPF_6$ in EC: DMC (LB-301, China) is selected as the electrolyte and Celgard 2400 as the separator. The galvanostatic charge/discharge performance of the cell was evaluated at a constant rate of 0.1 C by a cell testing instrument (LAND CT2001A) in the potential range of 3.0 to 4.3 V (vs Li/Li^+). The cyclic voltammetry curve and electrochemical impedance spectrum were measured by a potentiostat/galvanostat (EG&G PAR273A) and 5210 Lock-in Amplifier. The cyclic voltammetry curve was measured at a scanning rate of 0.1 mV s^{-1}. The impedance spectrum was measured by applying a small ac signal with and without overlapping a dc voltage. The frequency range used in the impedance measurement was between 10 mHz and 100 kHz. The ac amplitude was 5 mV and the dc voltage was 4.2 V. The ac impedance spectra were simulated with equivalent circuits using Zview software.

The XRD patterns of $Li_3V_2(PO_4)_3$/C sintered at 1073 K and 1123 K (800 °C and 850 °C) are shown in Figures 1(b) and (c), respectively. All patterns can be indexed as monoclinic $Li_3V_2(PO_4)_3$ with a space group of $P2_1/n$.[30] No peaks relating to other secondary phases were observed. $Li_3V_2(PO_4)_3$ has two different phases, i.e., the thermodynamically stable monoclinic phase and the rhombohedral phase which exists only under special conditions.[34,35] The monoclinic lithium vanadium phosphate is considered to have better electrochemical performances than the rhombohedral phase.[35] Compared with powders sintered at 1073 K (800 °C), $Li_3V_2(PO_4)_3$/C sintered at 1123 K (850 °C) had narrower peaks. The grain size values of both samples were analyzed using Scherrer's equation and were measured to be 32 nm for 1073 K (800 °C) and 45 nm for 1123 K (850 °C), respectively. The increase in sintering temperature leads to coarsening of crystalline grains. No peak related to carbon was observed due to the low carbon content in the composites, which is measured to be 3.89 pct for the sample sintered at 1073 K (800 °C) and 3.86 pct for the sample sintered at 1123 K (850 °C) by carbon-sulfur analyzer. SEM images of $Li_3V_2(PO_4)_3$/C sintered at 1073 K and 1123 K (800 °C and 850 °C) are presented in Figure 2. $Li_3V_2(PO_4)_3$/C sintered at both 1073 K and 1123 K (800 °C and 850 °C) consists of irregularly aggregated microsize solid particles. The powders sintered at 1123 K (850 °C) are more heavily aggregated than those sintered at 1073 K (800 °C).

The first cycle charge/discharge curves and the discharge cyclic performance of $Li_3V_2(PO_4)_3$/C cathodes sintered at 1073 K and 1123 K (800 °C and 850 °C) for Li
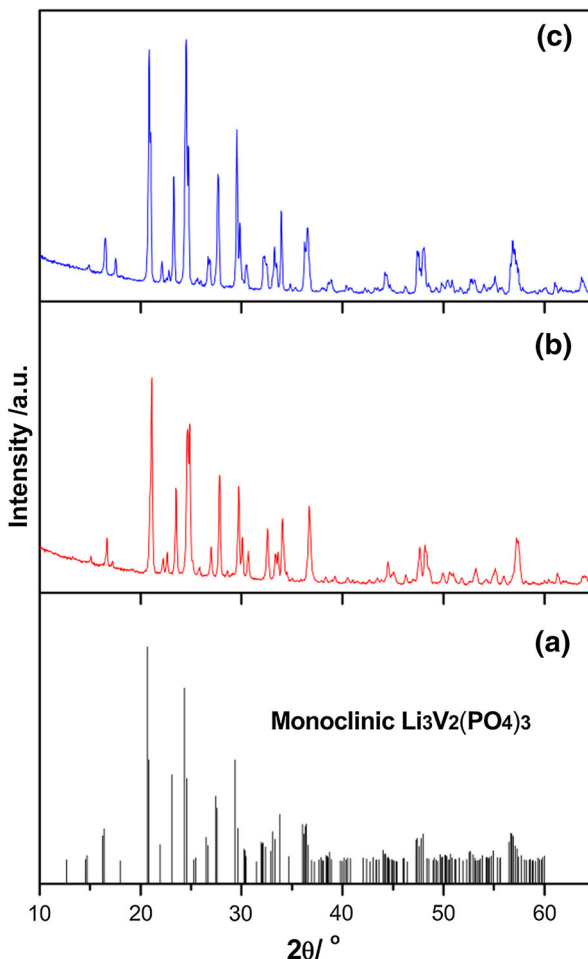

Fig. 1—XRD results of $Li_3V_2(PO_4)_3$/C: (a) standard patterns, and sintered at (b) 1073 K (800 °C), and (c) 1123 K (850 °C), respectively.

ion batteries at the rate of 0.1 C are presented in Figures 3(a) and (b), respectively. It can be seen that the sintering temperature significantly affects the electrochemical performance of $Li_3V_2(PO_4)_3$/C cathodes for Li ion batteries. In the potential range of 3.0 to 4.3 V, the first cycle charge/discharge capacity of the $Li_3V_2(PO_4)_3$/C cathode sintered at 1073 K (800 °C) is 113.4/111.5 mAh g^{-1} and then increased to 126.7/121.3 mAh g^{-1} when sintered at 1123 K (850 °C) which approaches its theoretical capacity of 133 mAh g^{-1}.[33] It is comparable with the capacity of $Li_3V_2(PO_4)_3$/C cathode synthesized by the microwave-assisted hydrothermal method followed by a post annealing process.[9] The $Li_3V_2(PO_4)_3$/C delivered the first discharge capacity of 128.5 mAh g^{-1} at 0.1 C rate in the voltage range of 3.0 to 4.3 V and low capacity in ion liquid electrolytes.

Both $Li_3V_2(PO_4)_3$/C cathodes show three charge/discharge potential plateaus (Figure 3(a)), which are related to three reversible Li ion intercalation/extraction steps (1) to (3), and a high capacity retention rate after 100 cycles (Figure 3(b)). The capacity retention of the $Li_3V_2(PO_4)_3$/C cathode sintered at 1123 K (850 °C) is as high as 97.3 pct.

With increase in the sintering temperature, the plateau potential decreased during the charge process and
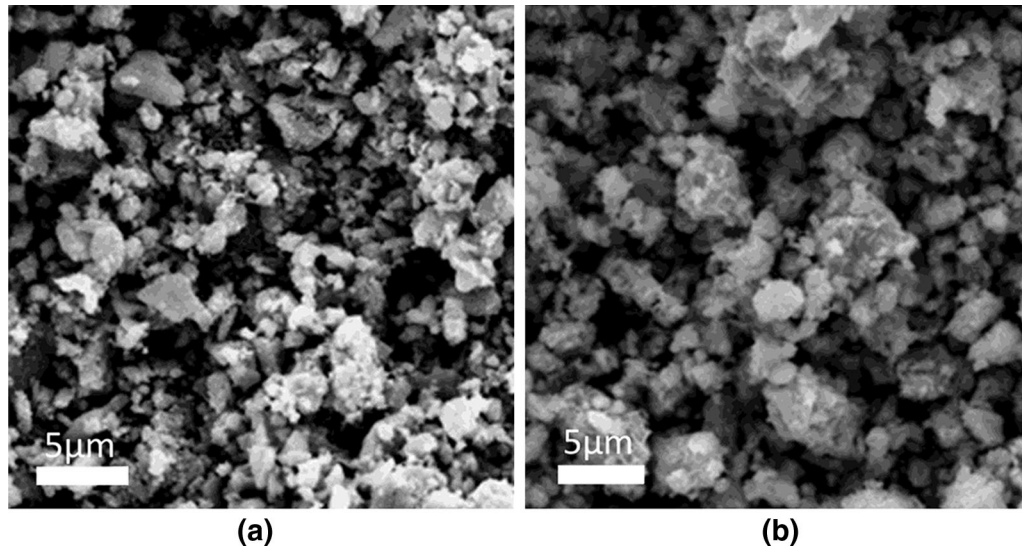
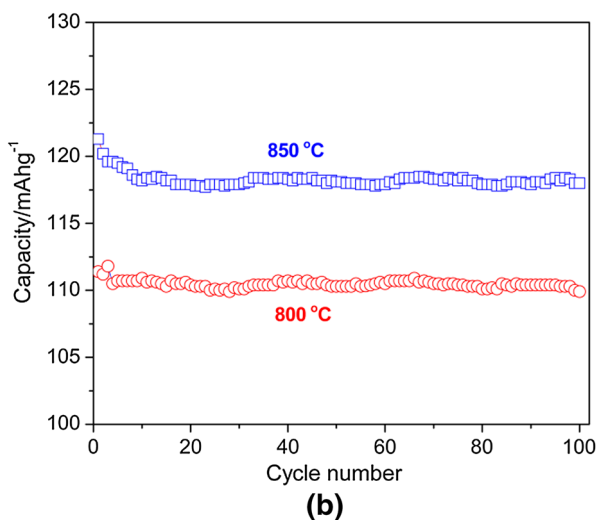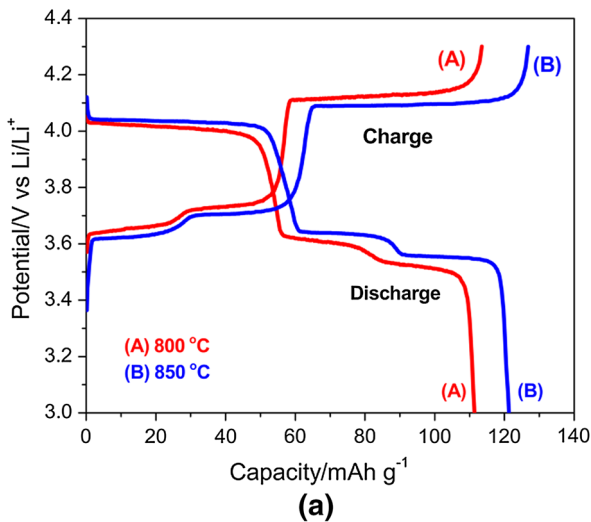Fig. 2—SEM images of Li$_3$V$_2$(PO$_4$)$_3$/C sintered at (*a*) 1073 K (800 °C) and (*b*) 1123 K (850 °C).

(a)

(b)

Fig. 3—(*a*) The first cycle charge/discharge and (*b*) the discharge cyclic performance of Li$_3$V$_2$(PO$_4$)$_3$/C cathode for Li ion batteries.

Table I. The Charge/Discharge Plateau Potential (V) of Li$_3$V$_2$(PO$_4$)$_3$/C Cathodes for Li Ion Batteries

T [K (°C)] Potential (V)	[1073 K (800 °C)]		[1123 K (850 °C)]	
	Charge	Discharge	Charge	Discharge
Step (1)	3.66	3.52	3.63	3.56
Step (2)	3.73	3.60	3.70	3.64
Step (3)	4.12	4.02	4.09	4.04

increased during the discharge process, indicating a smaller resistance to the charge/discharge process for the cathode sintered at 1123 K (850 °C), as consistent with the previous report.[36] It is known that increase in the sintering temperature will coarsen the particles and increase their aggregations, which is not favorable for lithium insertion/extraction.[37] This smaller resistance to the charge/discharge process may be attributed to a stronger interaction at the interface between carbon and Li$_3$V$_2$(PO$_4$)$_3$ at a higher sintering temperature. The stronger interaction makes electron transfer between different phases easier, thus increasing the conductivity of active materials. The charge/discharge plateau potentials of both samples are listed in Table I.

Figure 4 shows the cyclic voltammetry curves of Li$_3$V$_2$(PO$_4$)$_3$/C cathodes sintered at 1073 K and 1123 K (800 °C and 850 °C), respectively. Both samples have three anodic peaks, denoted as A1, A2, A3, and cathodic peaks, denoted as C1, C2, and C3, which are related to the three insertion/extraction steps (1 to 3) in Li$_3$V$_2$(PO$_4$)$_3$/C cathodes. The anodic peaks of the sample sintered at 1123 K (850 °C) shifted in the direction of low potential, while the cathodic peaks in the direction of high potential compared with that sintered at 1073 K (800 °C), resulting in larger peak potential differences between charge and discharge at each step. In addition, Li$_3$V$_2$(PO$_4$)$_3$/C sintered at 1123 K (850 °C) shows a larger current value, which is consistent with its smaller resistance shown before. The large
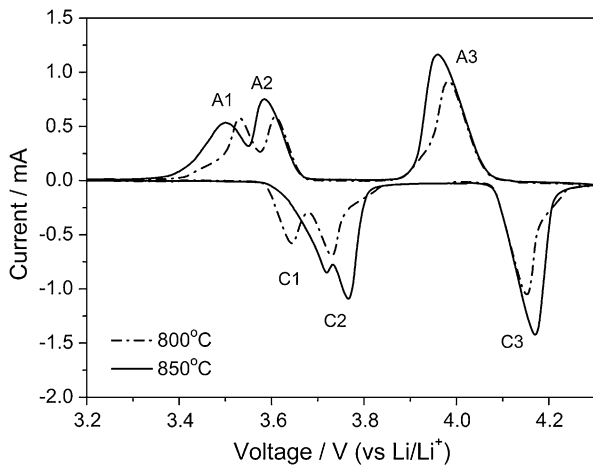
Fig. 4—Cyclic voltammetry curves of $Li_3V_2(PO_4)_3/C$ cathode for Li ion batteries.

current can lead to a higher degree of polarization (the degree of deviation from its equilibrium value of the electrode potential) of the cathode.[38] This explains why the sample sintered at 1123 K (850 °C) shows a larger potential difference.

Ac impedance spectrum is used to analyze the interfacial and internal electrical properties of the electrode. Simulation of ac impedance spectrum with equivalent circuit can show many kinetic parameters, such as charge transfer resistance (R_{ct}) in the interface of electrode and electrolyte, and Warburg impedance (Z_w) that is related to Li ion diffusion in the electrode. According to the cycle voltammetry curve of $Li_3V_2(PO_4)_3/C$ cathodes shown in Figure 4, Li ion insertion/extraction in the cathodes occurs at the potential range of 3.4 to 4.2 V. To investigate the resistance of Li ion insertion/extraction in the cathode, which is referred as the internal resistance (R_{in}), the dc voltage (4.2 V) between the lithium anode and $Li_3V_2(PO_4)_3/C$ cathode was overlapped with a small ac signal of 5 mV during the ac impedance spectra measurement of the cathode. It is reported that Wang et al investigated the ac impedance spectrum of TiO_2 cathode in $CaCl_2$ molten salt by overlapping a dc voltage greater than its decomposition potential.[39] The electro-deoxidation steps and resistance of TiO_2 in molten $CaCl_2$ were analyzed.[39] The charge transfer between the ferri/ferrocyanide redox couple and poly(3,4-ethylenedioxythiophene) electrodes was also investigated by electrochemical impedance spectroscopy at different dc potentials with different ratios of $Fe(CN)_3^{-6}$:$Fe(CN)_4^{-6}$ in solutions.[40]

Figure 5 shows the electrochemical impedance spectra of $Li_3V_2(PO_4)_3/C$ cathodes without overlapping dc voltage (Figure 5(a)) and with the dc voltage of 4.20 V (Figure 5(b)) and the equivalent circuits. The electrochemical impedance spectra without overlapping dc voltage are composed of small intercepts with the x-axis at the highest frequency of 100 kHz, semicircles at the high frequency range, and straight lines at the low frequency range, which corresponds to the electrolyte resistance (R_s), charge transfer resistance (R_{ct}), and a constant phase angle element (CPE), as well as Warburg

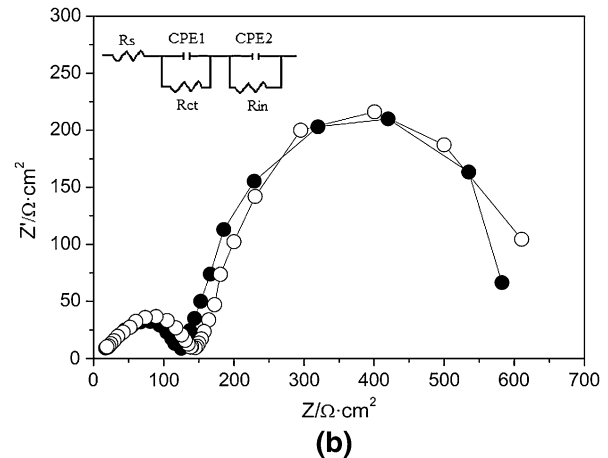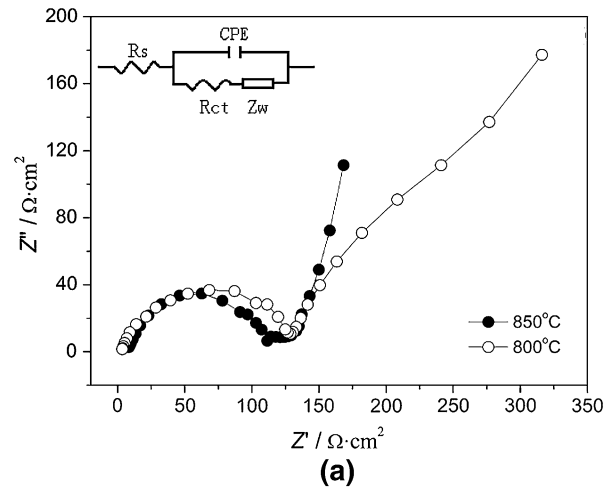(a)

(b)

Fig. 5—Electrochemical impedance spectra of $Li_3V_2(PO_4)_3/C$ cathode for Li ion batteries (a) without overlapping dc voltage and (b) with the dc voltage of 4.2 V.

impedance (Z_w). Warburg impedance is related to electrode intrinsic resistance. Note that both the semicircle and the length of the straight line in the impedance spectrum of $Li_3V_2(PO_4)_3/C$ cathodes sintered at 1123 K (850 °C) are smaller than those sintered at 1073 K (800 °C). This observation proves that the sample sintered at 1123 K (850 °C) has small charge transfer resistance and electrode intrinsic resistance. The almost linear response of the impedance spectra in the low frequency region indicates that diffusion of Li ions in the cathodes is slow and is the rate controlling step of the charge/discharge process.

Table II lists the fitted equivalent circuit parameters of the impedance spectra shown in Figure 5(a). The values of R_{ct}, CPE, and Z_w of $Li_3V_2(PO_4)_3/C$ cathode sintered at 1123 K (850 °C) are 0.63, 0.26, and 0.74 times of the $Li_3V_2(PO_4)_3/C$ cathode sintered at 1073 K (800 °C), respectively, further confirming that $Li_3V_2(PO_4)_3/C$ cathode sintered at 1123 K (850 °C) is of excellent electrical and electrochemical properties for Li ion battery.

The ac impedance spectra of $Li_3V_2(PO_4)_3/C$ cathodes with dc voltage overlapped (Figure 5(b)) have the different shapes from those without dc voltage

Table II. The Fitted Equivalent Circuit Parameters of the Impedance Spectra

T [K (°C)]	R_s (Ω cm^2)	R_{ct} (Ω cm^2)	CPE (F cm^2)	Z_w (Ω cm^2)
1073 K (800)	3.8	130.9	0.047	389.6
1123 K (850)	4.9	82.5	0.012	287.0

(Figure 5(a)), because of the Li ion insertion/extraction in the cathodes at the dc voltage of 4.2 V. The first semicircles of the ac impedance spectra in the high frequency range are related to the charge transfer resistance (R_{ct}) and the interfacial double layer capacitive property (CPE1). These two parameters are close in magnitude to their counterparts in the ac impedance spectra with potential overlapped. The second semicircles in the low frequency range, as shown in Figure 5(b), are related to the internal resistances (R_{in}) and capacitive property (CPE2) of Li ion insertion/extraction process in the cathode. The value of R_{in} is much greater than R_{ct} for both cathodes sintered at different temperatures, while the cathode sintered at 1123 K (850 °C) shows smaller charger transfer resistance and internal resistance. By simulating the ac impedance spectra with the equivalent circuit shown in Figure 5(b), the internal resistances for the cathodes sintered at 1073 K and 1123 K (800 °C and 850 °C) are 506.4 and 572.1 Ω cm^2, respectively.

To conclude, the charge transfer resistance of Li$_3$V$_2$(PO$_4$)$_3$/C cathode and the internal resistance of Li ion insertion/extraction in the cathode during the charge/discharge process are investigated by ac impedance spectrum. The internal resistance of 506.4 to 572.1 Ω cm^2 is much greater than the charge transfer resistance. The Li$_3$V$_2$(PO$_4$)$_3$/C cathode sintered at 1123 K (850 °C) exhibited excellent physicochemical performances with small electrode intrinsic resistance, charge transfer resistance, and internal resistance. It showed a first charge/discharge capacity of 126.7/121.3 mAh g^{-1} and a high capacity retention rate of 97.3 pct after 100 charge/discharge cycles in the potential range of 3.4 to 4.2 V. This work reveals the Li ion insertion/extraction resistance *via* a novel approach and improves the fundamental understanding of the charge/discharge process of Li$_3$V$_2$(PO$_4$)$_3$/C cathodes in Li ion batteries.

REFERENCES

1. C.-M. Park, J.-H. Kim, H. Kim, and H.-J. Sohn: *Chem. Soc. Rev.*, 2010, vol. 39, pp. 3115–41.
2. S.-Y. Chung, J.T. Bloking, and Y.-M. Chiang: *Nat. Mater.*, 2002, vol. 1, pp. 123–28.
3. M.Y. Saidi, J. Barker, H. Huang, J.L. Swoyer, and G. Adamson: *J. Power Sour.*, 2003, vol. 119, pp. 266–72.
4. Y.Q. Qiao, X.L. Wang, Y. Zhou, J.Y. Xiang, D. Zhang, S.J. Shi, and J.P. Tu: *Electrochim. Acta*, 2010, vol. 56, pp. 510–16.
5. X.H. Rui, Y. Jin, X.Y. Feng, L.C. Zhang, and C.H. Chen: *J. Power Sour.*, 2011, vol. 196, pp. 2109–14.
6. Y. Li, Z. Zhou, M. Ren, X. Gao, and J. Yan: *Electrochim. Acta*, 2006, vol. 51, pp. 6498–02.
7. C. Chang, J. Xiang, X. Shi, X. Han, L. Yuan, and J. Sun: *Electrochim. Acta*, 2008, vol. 54, pp. 623–27.
8. H. Wang, Y. Liar, C. Huang, Y. Zhong, and S. Liu: *J. Power Sour.*, 2012, vol. 208, pp. 282–87.
9. J.T. Xu, S.L. Chou, C.F. Zhou, Q.F. Gu, H.K. Liu, and S.X. Dou: *J. Power Sour.*, 2014, vol. 246, pp. 124–31.
10. S.L. Wang, Z.X. Zhang, S.H. Fang, L. Yang, C.C. Yan, and S.I. Hirano: *Electrochim. Acta*, 2013, vol. 111, pp. 685–90.
11. H. Huang, S.C. Yin, T. Kerr, N. Taylor, and L.F. Nazar: *Adv. Mater.*, 2002, vol. 14, pp. 1525–28.
12. M.M. Ren, Z. Zhou, X.P. Gao, W.X. Peng, and J.P. Wei: *J. Phys. Chem. C*, 2008, vol. 112, pp. 5689–93.
13. P.G. Bruce, B. Scrosati, and J. Tarascon: *Angew. Chem. Int. Ed.*, 2008, vol. 47, pp. 2930–46.
14. A.S. Arico, P. Bruce, B. Scrosati, J.-M. Tarascon, and W. Van Schalkwijk: *Nat. Mater.*, 2005, vol. 4, pp. 366–77.
15. D. Ai, K. Liu, Z. Lu, M. Zou, D. Zeng, and J. Ma: *Electrochim. Acta*, 2011, vol. 56, pp. 2823–27.
16. M. Ren, Z. Zhou, Y. Li, X.P. Gao, and J. Yan: *J. Power Sour.*, 2006, vol. 162, pp. 1357–62.
17. B. Jiang, S. Hu, M. Wang, X. Ouyang, and Z. Gong: *Rare Met.*, 2011, vol. 30, pp. 115–19.
18. Y.G. Mateyshina and N.F. Uvarov: *J. Power Sour.*, 2011, vol. 196, pp. 1494–97.
19. C. Dai, Z. Chen, H. Jin, and X. Hu: *J. Power Sour.*, 2010, vol. 195, pp. 5775–79.
20. J.S. Huang, L. Yang, K.Y. Liu, and Y.F. Tang: *J. Power Sour.*, 2010, vol. 195, pp. 5013–18.
21. Q. Kuang, Y. Zhao, X. An, J. Liu, Y. Dong, and L. Chen: *Electrochim. Acta*, 2010, vol. 55, pp. 1575–81.
22. C. Deng, S. Zhang, S.Y. Yang, Y. Gao, B. Wu, L. Ma, B.L. Fu, Q. Wu, and F.L. Liu: *J. Phys. Chem. C*, 2011, vol. 115, pp. 15048–56.
23. M. Bini, S. Ferrari, D. Capsoni, and V. Massarotti: *Electrochim. Acta*, 2011, vol. 56, pp. 2648–55.
24. Q. Kuang, Y. Zhao, and Z. Liang: *J. Power Sour.*, 2011, vol. 196, pp. 10169–75.
25. J. Yan, W. Yuan, H. Xie, Z. Tang, F. Liu, W. Mao, Q. Xu, and X. Zhang: *J. Solid State Electrochem.*, 2012, vol. 16, pp. 3201–06.
26. W. Yuan, J. Yan, Z. Tang, O. Sha, J. Wang, W. Mao, and L. Ma: *Electrochim. Acta*, 2012, vol. 72, pp. 138–42.
27. L.-L. Zhang, G. Liang, G. Peng, F. Zou, Y.-H. Huang, M.C. Croft, and A. Ignatov: *J. Phys. Chem. C*, 2012, vol. 116, pp. 12401–08.
28. E. Kobayashi, A. Kitajou, S. Okada, and J.I. Yamaki: *J. Power Sour.*, 2013, vol. 244, pp. 312–17.
29. X.H. Rui, Q.Y. Yan, S.K. Maria, and T.M. Lim: *J. Power Sour.*, 2014, vol. 258, pp. 19–38.
30. X.H. Rui, C. Li, and C.H. Chen: *Electrochim. Acta*, 2009, vol. 54, pp. 3374–80.
31. G. Yang, H.D. Liu, H.M. Ji, Z.Z. Chen, and X.F. Jiang: *Electrochim. Acta*, 2010, vol. 55, pp. 2951–57.
32. Q.Q. Chen, J.M. Wang, Z. Tang, W.C. He, H.B. Shao, and J.Q. Zhang: *Electrochim. Acta*, 2007, vol. 52, pp. 5251–57.
33. H. Liu, P. Gao, J. Fang, and G. Yang: *Chem. Commun.*, 2011, vol. 47, pp. 9110–12.
34. S.C. Yin, H. Grondey, P. Strobel, M. Anne, and L.F. Nazar: *J. Am. Chem. Soc.*, 2003, vol. 125, pp. 10402–11.
35. S.C. Yin, P.S. Strobel, H. Grondey, and L.F. Nazar: *Chem. Mater.*, 2004, vol. 16, pp. 1456–65.
36. P. Fu, Y. Zhao, Y. Dong, X. An, and G. Shen: *J. Power Sour.*, 2006, vol. 162, pp. 651–57.
37. A. Andersson and J.O. Thomas: *J. Power Sour.*, 2001, vol. 97, pp. 498–502.
38. A.V. Virkar, J. Chen, C.W. Tanner, and J.-W. Kim: *Solid State Ionics*, 2000, vol. 131, pp. 189–98.
39. S.L. Wang and Y.J. Li: *J. Electroana. Chem.*, 2004, vol. 571, pp. 37–42.
40. F. Sundfors and J. Bobacka: *J. Electroana. Chem.*, 2004, vol. 572, pp. 309–316.